# SUPPLEMENTAL MATERIAL

Suckau *et al.*

**Chronic Cardiac-Targeted RNA Interference for the Treatment of Heart Failure Restores Cardiac Function and Reduces Pathological Hypertrophy**

## SUPPLEMENTAL METHODS

### Development of Recombinant Adenoviral and AAV Vectors

Recombinant Adeno-Associated Virus (rAAV) vectors were developed for the *in vitro* studies as pseudotyped rAAV6 and for the *in vivo* work as rAAV9. Both contained identical AAV2 vector genomes with the indicated shRNA expression cassettes and were processed identically with the exception of using the plasmid AAV6cap for rAAV6 and AAV9cap for rAAV9, respectively. Throughout all *in vitro* and *in vivo* studies we used only self-complementary ("dimeric") rAAV genomes due to their enhanced performance compared to single-stranded ("monomeric") rAAV vectors. Starting from an shRNA expression cassette previously used in an adenoviral (AdV) vector AdV-shPLB, which efficiently and stably silenced PLB expression in cultured primary neonatal rat cardiomyocytes (NRCMs) [1], we sought to develop AdV and rAAV vectors co-expressing shRNA and GFP as a marker which would allow vector tracking during the experiment with heart failure (HF) animals by *in vivo* imaging. However, a construct rAAV-shPLB-CMV-GFP displayed very low silencing activity compared to the original AdV-shPLB vector which contained no CMV-GFP component (**Fig. 1*a***). The rAAV vector produced GFP under CMV control with transcription in the CMV-GFP cassette running opposite to the U6-promotor-shRNA cassette. To test if the CMV promoter itself and/or the GFP sequence were responsible for the loss of silencing activity, we constructed the vector rAAV-shPLB-CMV-β-intron with an intronic "stuffer" sequence instead of the GFP. Both rAAV-shPLB-CMV-GFP (size 2.40 kb) and rAAV-shPLB-CMV-β-intron (size 2.14 kb) had sizes considered necessary for packaging into the capsid. A third vector which contained neither CMV nor GFP or β-intron, but only the original U6-shPLB cassette from AdV-PLB, rendered at total vector genome size of only 0.98 kb. Nevertheless this "minimalistic" rAAV-shPLB was efficiently packaged during the standard procedure, probably as a concatemer (data not shown). The maps of these 4 and of 2 additional control vectors (rAAV-shPLB-GFP and rAAV-shPLB-β-intron) are summarized in **Fig. 1*a***.

### Virus Vector Production and Purification

rAAV9-shGFP and rAAV9-shPLB were produced using the two-plasmids protocol described by Zolotukhin *et al*. 1999 [2] with the following modifications: 293-T cells (*ATCC, Manassas, VA*) were grown in triple flasks for 24 h (DMEM, 10% FBS) prior to adding the calcium phosphate precipitate. After 72 hours, the virus was purified from benzonase-treated cell crude lysates over an iodixanol density gradient (*Optiprep, Greiner Bio-One Inc., Longwood, FL*), followed by heparin-agarose type I affinity chromatography (*Sigma-Aldrich Inc., St. Louis, MO*). Finally viruses were concentrated and formulated into lactated Ringer's solution (*Baxter Healthcare Corporation, Deerfield, IL*) using a Vivaspin 20 Centrifugal concentrators 50K MWCO (*Vivascience Inc., Carlsbad, CA*), and stored at –80$^{o}$C.

**Vector Quality Assessment and Titration**

Vector stock biochemical purity (>95%) was assessed by silver staining after electrophoresis. Genome containing particles (gcp) were determined by a real-time PCR approach (*LightCycler, Roche Diagnostics*) using the SYBR™ Green Taq ReadyMix™ (*SIGMA, Saint-Louis, MO*) and primers CMV-F and CMV-R.

**Vector Evaluation in Primary Cardiomyocytes**

Primary neonatal cardiomycytes (NRCMs) are suitable to pre-test any RNAi-based cardiac therapy before its definitive test *in vivo* since, although developmentally regulated, the SERCA2a/PLB system functions well in NRCMs and adenoviral gene transfer strategies targeting the SERCA2a/PLB system were successful in both neonatal and adult cardiomyocytes. Although both cell types are well suited for *in vitro* pre-testing, a number of other differences between cultured cardiomyocytes and the intact heart *in vivo* render any *in vitro* study of RNA-based therapies in cultured cells rather preliminary.

*Cell cultures*: Primary neonatal cardiomyocytes (NRCMs) were prepared from ventricular tissue of 1-3 day-old Wistar rat pups. NRCMs were grown in 6-well dishes.

*Evaluation of phospholamban silencing*: PLB mRNA and protein expression in NRCMs and rat hearts, as well as SERCA2a and NCX protein in rat hearts, was determined by Northern and Western blot analyses as described [1, 3, 4, 5].

*Calcium Transients During RNAi Treatment:* $[Ca^{2+}]_i$ transients were measured during electrical stimulation at 1 Hz after loading of NRCMs with 8 µM Fluo-4/AM for 20 min (image capture at 120 Hz, 8.3 ms per image). Five treatment groups of NRCMs (number of cells) were studied: AAV9-shPLB (n=26), AAV9-shGFP (n=26), AdV-shPLB (n=71), AdV-shGFP (n=49), and untreated control cells (n=32). The amplitude of the transient (systolic $[Ca^{2+}]$ ($F/F_0$)), its time to peak (TTP) (ms), and the time constant $\tau$ of its decay (ms) were measured. The measurement of $[Ca^{2+}]_i$ transients during AAV9-shPLB treatment of NRCMs (**Fig. 1*e,f***) showed that this vector led to significantly higher amplitude and accelerated transient kinetics (with shortened TTP and $\tau$) compared to the AAV9-shGFP group with transients indistinguishable from untreated cells. AdV-shPLB treatment also resulted in a significantly higher amplitude compared to the AdV-shGFP group. In contrast to the AAV9 groups, however, the TTP was prolonged in AdV-shPLB *vs*. AdV-shGFP and there was no difference in $\tau$. Therefore additional studies of sarcoplasmic reticulum (SR) $Ca^{2+}$ loading in the AdV groups (**Suppl. Fig. 1*d***) were performed as follows: $[Ca^{2+}]_i$ transients were again measured during electrical stimulation at 1 Hz after loading of NRCMs with 8 µM Fluo-4/AM for 20 min, but followed by rapid addition of 20 mM caffeine which blocks re-uptake of $Ca^{2+}$ into the SR *via* SERCA2a. Electrically stimulated $[Ca^{2+}]_i$ transients were compared with the caffeine-induced and the fractional release of $Ca^{2+}$ was calculated (see Kockskämper et al. 2008 [6] and references therein).

*Induction of hypertrophy*: Phenylephrine (PE) at a concentration of 100 µM was employed in part of the *in vitro* studies as a hypertrophic stimulus. *TaqMan* assays to quantitate the cellular miRNAs were performed in NRCMs under baseline conditions (**Suppl. Fig. 4*a***) or in the presence of PE (**Suppl. Fig. 4*b***). The agent was added on day 2 of culture, either alone or together with the respective RNAi vector. NRCM cultures were continued in the presence of 10% FACS.

**Quantitation of Gene Expression and shRNA Production by *TaqMan*™ Assays**

*microRNA assays*: miRNAs were isolated from cells and tissues by using the Mirvana RNA isolation kit according to the instructions of the manufacturer (Ambion, Austin, TX, USA). In a search for possible influences of vector-derived shRNAs on cardiomyocyte miRNAs we used *TaqMan*™ assays to quantitate (**Suppl. Fig. 4*a-c***) two miRNAs (miRNA-1, miRNA-133a) known to be functionally expressed in the heart [7-9]. *BNP assay:* Cardiac BNP gene expression was likewise quantitated by *TaqMan*™ in the hearts of vector-treated rats (**Suppl. Fig. 3*e***). *shPLB production*: The quantitation of *short hairpin* RNA transcription by the different RNAi vectors (**Fig. 1*c***) followed a previously published protocol [1, 10].

**Transaortic Banding**

Four-week old Sprague Dawley rats (70-80 g) were anesthetized with intraperitoneal pentobarbital (65 mg/kg) and placed on a ventilator. A suprasternal incision was made exposing the aortic root and a tantalum clip with an internal diameter of 0.58 mm (*Weck, Inc.*) was placed on the ascending aorta. Animals in the sham group underwent a similar procedure without insertion of a clip. The supra-clavicular incision was then closed and the rats were transferred back to their cages. The supra-clavicular approach was performed because during gene delivery a thoracotomy is necessary and by not opening the thorax during the initial aortic banding, avoids adhesions when gene delivery is performed.

Animals were initially divided into two groups: one group of 56 animals with transaortic aortic banding (TAB) and a second group of 12 animals which were sham-operated (10 of the sham operated animals survived). In the animals which were aortic banded we waited 25-30 weeks for the animals to develop left ventricular dilatation and a decrease in ejection fraction by 25% prior to cardiac gene transfer. From the initial 56 who underwent pressure overload hypertrophy only 40 animals survived and were further divided to receive either Ad-shGFP (n=10) or Ad-shPLB (n=10), or rAAV9-shGFP (n=10) or rAAV9-shPLB (n=10).

**Serial Echocardiographic Assessment**

After twenty-two weeks of banding, serial echocardiograms were performed on a weekly basis in lightly anesthetized animals (pentobarbital 40 mg/kg intra-peritoneally). Transthoracic M-mode and two-dimensional echocardiography was performed with a *GE Vivid-7* ultrasound machine and a 12 MHz broadband transducer. A mid-papillary level left ventricular short axis view was used and measurements of posterior wall thickness, left ventricular diastolic dimension and fractional shortening were collected. Gene transfer was performed in all animals within 3 days of detection of a drop in fractional shortening (FS) of > 25% compared to FS at 12 weeks post-banding. The operators performing the echocardiographic studies were blinded in terms of the animal groups they were studying.

**Cardiac Distribution of AAV9 Vectors After Intravenous Injection**

Rats were injected intravenously (i.v.) either with a marker vector rAAV9-GFP which expresses the marker protein GFP, or with saline. 1 month following delivery of rAAV9-GFP or saline the hearts were

removed and visualized under a fluorescent system (*Maestro In Vivo Imaging, Woburn, MA*) at 510 nm with single excitation peak at 490 nm of blue light (**Fig. 2*b,c***) shows the images observed.

In addition to this visualization of GFP expression at the macroscopic scale, GFP immunhistochemical staining was performed 1 month after i.v. injection of rAAV9-GFP to evaluate its distribution at microscopic dimensions (**Fig. 2*d***, **Suppl. Fig. 2*a,b***). After blockade of endogenous peroxidase with 30% hydrogen peroxide, washing in PBS buffer, a polyclonal rabbit-anti-hrGFP antibody (*Vitality ™, catalogue #240142, Stratagene*) was added in 1:1.000 dilution for 120 min. After washing, as secondary a polyclonal goat-anti-rabbit immunoglobulins/HRP antibody (*catalogue# P0448, Dako, Glostrup, Denmark*) was used in 1.50 dilution for 60 min. Staining and counterstaining with haemalaun was as described [11].

For Western blot analysis of GFP expression in the different organs the polyclonal rabbit-anti-hrGFP antibody (*Vitality ™, catalogue #240142 Stratagene*) was used in 1:5.000 dilution at 4°C overnight. As secondary the polyclonal goat-anti-rabbit immunoglobulins/HRP antibody (*catalogue# P0448, Dako, Glostrup, Denmark*) was used in 1:2.000 dilution at RT for 60 min. For detection of GAPDH as loading control a monoclonal mouse-anti-GAPDH antibody (*catalogue# MAB374, Chemicon /Millipore*) was used as primary in 1:5.000 dilution for 1 hr at RT, and a polyclonal goat-anti-mouse immunoglobulins/ HRP antibody (*catalogue# P0447, Dako, Glostrup, Denmark*) as secondary in 1:10.000 dilution at 1 hr at RT. The GFP Western blots all organs were processed equally as described, then developed by use of a chemiluminescence kit (*USB Corp., Cleveland, OH*). Blots were then exposed to X-ray film for 5 min each. For densitometric quantitation of the films *TINA 2.09* software and a *Raytest* ™ system were used.

**Experimental Protocol for RNA Interference Therapy *in vivo***

The adenoviral delivery system has previously been described by our group in detail [4, 5, 12-14]. Briefly, after anesthetizing the rats and performing a thoracotomy, a 22 G catheter containing 200 μl of adenoviral ($3x10^{10}$ pfu) solution was advanced from the apex of the left ventricle to the aortic root. The aorta and main pulmonary artery were clamped for 40 sec distal to the site of the catheter and the solution injected, then the chest was closed and the animals were allowed to recover. For experiments with rAAV9, a simple tail vein injection was performed using $5x10^{11}$ genomes of either rAAV9-shRNA vector. Animals in the sham group were injected with saline.

**Hemodynamics Evaluation during RNA Interference Therapy**

Rats in the different treatment groups and at different stages following adenoviral gene transfer were anesthetized with 40 mg/kg of pentobarbital and mechanically ventilated. The chest was then opened through a mid-line incision and the heart exposed. A small incision was then made in the apex of the left ventricle and a 2.0 French high fidelity pressure transducer (*MILAR Instruments Inc., TX*) introduced into the left ventricle. Pressure measurements were digitized at 1 KHz and stored for further analysis. Left ventricular systolic pressure (LVSP), end-diastolic left ventricular pressure (LVDP), the maximal rates of pressure rise (+dP/dt) and of pressure fall (-dP/dt), and the time constant of relaxation (t) were measured or derived in the different groups. The time course of isovolumic relaxation was measured using the equation: $P=P_o e^{-t/t} + P_B$, where P is the left ventricular isovolumic

pressure, $P_o$ is pressure at the time of peak -dP/dt and $P_B$ is residual pressure. The operators performing the hemodynamic studies were blinded in terms of the animal groups they were studying.

**Histology of Hearts after RNA Interference Therapy**

*Cardiomyocyte size and cardiac fibrosis*: Histological analyses were performed on a subset of animals to evaluate myocyte size (CMD) and collagen content (CAP). LV specimens were fixed with 10% formalin and embedded in paraffin. Sections (3 μm-thick) were stained with hematoxylin-eosin to determine CMD or with Azan-Mallory to assess CAP. In longitudinally oriented cardiomyocytes, transnuclear width was measured as CMD (**Fig. 3*f*** ). Digital photographs were taken at six sites on each Azan-Mallory section. Interstitial/perivascular collagen area and myocyte area were determined separately by counting the computerized pixels using an NIH imager (**Fig. 3*e*** ).

**Statistical Analysis**

Data in **Fig. 1*cf***, **2*g***, **3*a-f*** and in **Suppl. Fig. 1*ae***, **3*a-e*, 4*a-c*** are presented as mean (columns) ± SD (error bars).

We analyzed the groups of rats intervened on by using a two step procedure. First, we carried out an over-all F test to determine if there is any significant difference existing among any of the means. We then selected two means and calculated Tukey's test for each mean comparison. We then checked to see if Tukey's score is statistically significant with Tukey's probability/critical values.

Statistical significance was accepted at the level of $p<0.05$.

**References**


**1.** Fechner H, Suckau L, Kurreck J, Sipo I, Wang X, Pinkert S, Loschen S, Rekittke J, Weger S, Dekkers D, Vetter R, Erdmann V, Schultheiss H-P, Paul M, Lamers J, Poller W. Highly efficient and specific modulation of cardiac calcium homeostasis by adenovector-derived short hairpin RNA targeting phospholamban. *Gene Therapy.* 2007;14:211-218.

**2.** Zolotukhin S, Byrne BJ, Mason E, Zolotukhin I, Potter M, Chesnut K, Summerford C, Samulski R, Muzyczka N. Recombinant adeno-associated virus purification using novel methods improves infectious titer and yield. *Gene Ther.* 1999;6:973-985.

**3.** Eizema K, Fechner H, Bezstarosti K, Schneider-Rasp S, van der Laarse A, Wang H, Schultheiss H-P, Poller W, Lamers J. Adenovirus-based phospholamban-antisense-mRNA expression as a novel approach to improve cardiac contractile dysfunction - Comparison of a constitutive viral *versus* an endothelin-1-responsive cardiac promoter. *Circulation.* 2000;101:2193-2199.

**4.** del Monte F, Harding S, Dec G, Gwathmey J, Hajjar R. Targeting phospholamban by gene transfer in human heart failure. *Circulation.* 2002;105:904-907.

**5.** Hajjar R, Schmidt U, Matsui T, Guerrero J, Lee K-H, Gwathmey J, Dec G, Semigran M, Rosenzweig A. Modulation of ventricular function through gene transfer *in vivo*. *Proceedings of the National Academy of Science USA.* 1998;95:5251-5256.

**6.** Kockskämper J, Seidlmayer L, Walther S, Hellenkamp K, Maier L, Pieske B. Endothelin-1 enhances nuclear $Ca^{2+}$ transients in atrial myocytes through Ins(1,4,5)P3-dependent $Ca^{2+}$ release from perinuclear $Ca^{2+}$ stores. *Journal of Cell Science.* 2008;121:186-195.

**7.** Zhao Y, Ransom JF, Li A, Vedantham V, von Drehle M, Muth A, Tsuchihashi T, McManus M, Schwartz R, Srivastava D. Dysregulation of Cardiogenesis, Cardiac Conduction, and Cell Cycle in Mice Lacking miRNA-1-2. *Cell.* 20 2007;129:303-317.

**8.** Yang B, Lin H, Xiao J, Lu Y, Luo X, Li B, Zhang Y, Xu C, Bai Y, Wang H, Chen G, Wang Z. The muscle-specific microRNA miR-1 regulates cardiac arrhythmogenic potential by targeting GJA1 and KCNJ2. *Nat Med.* 2007;13:486-491.

**9.** Care A, Catalucci D, Felicetti F, Bonci D, Addario A, Gallo P, Bang ML, Segnalini P, Gu Y, Dalton N, Elia L, Latronico M, Hoydal M, Autore C, Russo MA, Dorn G, 2nd, Ellingsen O, Ruiz-Lozano P, Peterson K, Croce C, Peschle C, Condorelli G. MicroRNA-133 controls cardiac hypertrophy. *Nat Med.* 2007;13:613-618.

**10.** Fechner H, Pinkert S, Wang X, Sipo I, Suckau L, Kurreck J, Dorner A, Sollerbrant K, Zeichhardt H, Grunert H, Vetter R, Schultheiss H, Poller W. Coxsackievirus B3 and adenovirus infections of cardiac cells are efficiently inhibited by vector-mediated RNA interference targeting their common receptor. *Gene Ther.* 2007;14:960-971.

**11.** Noutsias M, Fechner H, Jonge H, Wang X, Dekkers D, Houtsmuller A, Pauschinger M, Bergelson J, Warraich R, Yacoub M, Hetzer R, Lamers J, Schultheiss H, Poller W. Human Coxsackie-adenovirus-receptor is co-localized with Integrins $\alpha_v\beta_3$ and $\alpha_v\beta_5$ on the cardiomyocyte sarcolemma and upregulated in dilated cardiomyopathy - Implications for cardiotropic viral infections. *Circulation.* 2001;104:275-280.

**12.** Sakata S, Lebeche D, Sakata N, Sakata Y, Chemaly ER, Liang LF, Tsuji T, Takewa Y, Del Monte F, Peluso R, Zsebo K, Jeong D, Park WJ, Kawase Y, Hajjar R. Restoration of mechanical and energetic function in failing aortic-banded rat hearts by gene transfer of calcium cycling proteins. *J Mol Cell Cardiol.* 2007;42:852-861.

**13.** Sakata S, Lebeche D, Sakata Y, Sakata N, Chemaly ER, Liang L, Nakajima-Takenaka C, Tsuji T, Konishi N, del Monte F, Hajjar RJ, Takaki M. Transcoronary gene transfer of SERCA2a increases coronary blood flow and decreases cardiomyocyte size in a type 2 diabetic rat model. *Am J Physiol Heart Circ Physiol.* 2007;292:H1204-1207.

**14.** Sakata S, Lebeche D, Sakata Y, Sakata N, Chemaly ER, Liang LF, Padmanabhan P, Konishi N, Takaki M, del Monte F, Hajjar R. Mechanical and metabolic rescue in a type II diabetes model of cardiomyopathy by targeted gene transfer. *Mol Ther.* 2006;13:987-996.

**Supplemental Table**

| | | | | |
|---|---|---|---|---|
| Echocardiographic measures in rats after sham-surgery or aortic banding | | | | |
| | | | | |
| Treatment | PW, mm | LVDD, mm | LVSD, mm | FS, % |
| | | | | |
| Sham | | | | |
| 6 wk | 1.83 ± 0.12 | 8.15 ± 0.22 | 4.80 ± 0.22 | 41.4 ± 3.3 |
| 12 wk | 1.89 ± 0.11 | 8.32 ± 0.31 | 4.97 ± 0.28 | 44.2 ± 4.9 |
| 18 wk | 1.93 ± 0.10 | 8.55 ± 0.21 | 5.09 ± 0.25 | 40.1 ± 2.8 |
| 20 wk | 1.91 ± 0.10 | 8.61 ± 0.24 | 5.01 ± 0.24 | 41.4 ± 2.3 |
| LVH | | | | |
| 6 wk | 2.42 ± 0.16* | 7.93 ± 0.18 | 4.11 ± 0.21 | 46.8 ± 2.1* |
| 12 wk | 2.66 ± 0.14* | 8.44 ± 0.24 | 4.30 ± 0.16 | 48.2 ± 2.0* |
| 18 wk | 2.60 ± 0.18* | 8.87 ± 0.22* | 5.55 ± 0.13 | 36.4 ± 2.6* |
| 20-23 wk | 2.68 ± 0.20* | 9.44 ± 0.28* | 6.36 ± 0.10* | 32.6 ± 1.8* |
| | | | | |
| PW, posterior wall thickness during diastole; LVDD, left ventricular diameter during diastole; LVSD, left ventricular systolic diameter during systole; FS, fractional shortening; *, $P < 0.05$ compared to sham at similar time period; , $P < 0.05$ compared to values at 6 wk. From (Miyamoto et al, PNAS; 2000; Table 1; 97, Issue 2, 793-798 | | | | |

## Legends to Supplemental Figures

### Supplemental Fig. 1

### Interference of *CMV* promoter with *short hairpin* RNA Production

**A:** In addition to the recombinant adenoviral and rAAV vectors functionally characterized in **Fig. 1*a-c***, a direct comparison of the RNAi vectors rAAV6-shPLB-*CMV*-GFP (which contains a functional GFP expression cassette) *vs.* rAAV6-shPLB-GFP (carrying the GFP sequence but lacking a *CMV* promotor), and rAAV6-shPLB-*CMV*-β-intron (carrying β-intron plus *CMV* sequence) *vs.* rAAV-shPLB-β-intron (lacking the *CMV* promotor). Obviously, the presence of the CMV promoter *per se* reduced the shRNA production rate markedly, although shRNA suppression in the *CMV*-GFP marker vector was more pronounced.

**B:** Phase contrast (upper) and GFP fluorescence (lower) microphotograph of a cultured cardiomyocyte monolayer on day 5 after incubation with the rAAV6-shPLB-*CMV*-GFP marker vector, conforming a very high transduction rate for the rAAV6 pseudotype. Marker expression was obviously strong, so that transcription in *CMV*-GFP-bHG direction appears unaltered.

**C:** Synopsis of the structure of the vectors (see also **Fig. 1*a***) suggests as a possible cause for the disturbed shRNA production in the U6-shPLB-bGH direction a read-through from CMV through the termination signal into the very short shRNA sequence which then impairs proper formation of the *short hairpins* which mediate RNAi.

**D and E**: Measurement of $[Ca^{2+}]_i$ transients during AAV9-shPLB treatment of NRCMs (**Fig. 1*e,f***) showed that this vector led to significantly higher amplitude and accelerated transient kinetics (with a shortened TTP and $\tau$) compared to the AAV9-shGFP group with transients indistinguishable from untreated cells. AdV-shPLB treatment also resulted in a significantly higher amplitude compared to AdV-shGFP. In contrast to the AAV9 groups, TTP was prolonged in AdV-shPLB compared to the AdV-shGFP and there was no difference in $\tau$. Additional studies of the $[Ca^{2+}]_i$ transients induced by a caffeine pulse (upper panel **D**) revealed increased significantly ($p<0.05$) SR $Ca^{2+}$ loading and fractional $Ca^{2+}$ release (FR) from the SR in the AdV-shPLB compared to the AdV-shGFP group (lower panel **E**).

### Supplemental Fig. 2

### Expression of rAAV-GFP Vector After Intravenous Injection

**A:** Immunhistochemical staining for GFP in different organs 1 month after i.v. injection of rAAV9-GFP in rats. Whereas after i.v. injection of an adenoviral vector (AdV-GFP) no GFP was detectable within the heart (**Fig. 2*d***), rAAV9-GFP treatment resulted in strong cardiac GFP expression in 40-80% of cells (upper four photomicrographs) which is grossly homogeneous over large areas. Few areas are completely devoid of GFP immunoreactivity (encircled yellow), others show homogeneous cytoplasmic staining (encircled red). Staining is particularly dense at sites where high expression over 1 month has obviously resulted in the formation of precipitates (white arrows) of GFP which is stable in cells, in contrast to shRNA generated from RNAi vectors. AAn average of about 70% of cardiomyocytes was positive as assessed by GFP immunohistochemistry with variability of expression among individual

cells. The lower two photomicrographs document specificity of the GFP signal by lack of staining if the primary (GFP) antibody was omitted.

**B:** Immunhistochemical staining for GFP shows skeletal muscle (middle left) with faint staining of a major fraction of cells, whereas the liver (upper left) showed prominent signals of individual cells only. No signal was visible in the lungs (lower left). The photomicrographs on the right document specificity of the GFP signal by lack of staining without primary antibody.

**C:** This panel shows on the left side representative GFP Western blots of heart, liver, skeletal muscle and lung and respective GAPDH loading controls for liver and muscle. Side by side the results from two rats and two mice injected i.v. with rAAV9-GFP are shown. First, the high cardiac expression rate in both species is illustrated in contrast to the very faint expression in the lungs. Second, there was a difference in the GFP ratio heart/liver between rats (ratio ≈ 14.2) and mice (ratio ≈ 0.8), with relatively low hepatic GFP expression in rats. Third, there was a low level of skeletal muscle GFP expression in the rats, whereas no signal was detectable in mice. GFP Western blots processed and exposed by identical protocols were quantified by densitometric analysis as shown by the bar graphs below. In summary the data show that rAAV9-GFP resulted in a significantly higher heart/liver GFP expression ratio in rats than in mice. Cardiac affinity of rAAV9 vectors may apparently differ between species and appears to be favourable in rats over mice.

**Supplemental Fig. 3**

**Influence of RNAi Treatment on Hemodynamics and Cardiac Morphology**

**A:** *Influence of RNAi Therapy on Diastolic Function.* The figure summarizes the influence of the RNAi therapies upon hemodynamic parameters of diastolic LV function. The high LV filling pressure (LVEDP) in HF rats after TAC was significantly lowered by the shPLB vectors (lanes 3, 5) compared to the shGFP control vector groups (lanes 2, 4). The maximal rate of pressure fall (-dP/dt) was significantly increased by the shPLB vector therapies, as was also the isovolumetric relaxation time constant Tau. Values were restored to within the normal range (lanes 1) after three months of rAAV-shPLB therapy (lanes 5) (addendum to **Fig. 3*a***).

¶ denotes p<0.05 for animals treated with AdV-shPLB vs. control vector AdV-shGFP, ‡ denotes p<0.05 for treatment with rAAV9-shPLB vs. rAAV9-shGFP control group.

**B:** *Influence of RNAi Therapy on Systolic Function.* The figure summarizes RNAi treatment effects on systolic LV function analogous to panel A. Both the LV systolic pressure (LVSP) and the maximal rate of pressure rise (+dP/dt) were significantly improved by shPLB vector therapy (lanes 3, 5) compared to shGFP control vectors (lanes 2, 4). Echocardiography revealed an essentially normalized fraction shortening (FS) after 3 months of rAAV9-shPLB therapy (lane 5), whereas the improvement of FS was also significant but less pronounced for rats treated with AdV-shPLB (lane 3)(addendum to **Fig. 3*b***).

¶ denotes p<0.05 for animals treated with AdV-shPLB vs. control vector AdV-shGFP, ‡ denotes p<0.05 for treatment with rAAV9-shPLB vs. rAAV9-shGFP control group.

**C:** *Morphometric Changes During RNAi Therapy.* The figure summarizes the *post mortem* morphometry with marked LV hypertrophy induced by TAB (lanes 2, 4). LV weight and the LV/body weight (LV/BW) ratio rose ≈ 2/3 thirds above baseline (lanes 1). Treatment with either RNAi vector (lanes 3,

5) reduced this hypertrophy compared to the controls (lanes 2, 4) without reaching, however, the normal range. There was also a marked LV dilation as measured by the LV diameter/tibia length ratio. By morphometry the latter was reduced to within the normal range after 1 or 3 months of therapy with AdV-shPLB or rAAV9-shPLB (lanes 3, 5), respectively (addendum to **Fig. 3*c***).

¶ denotes p<0.05 for animals treated with AdV-shPLB vs. control vector AdV-shGFP, ‡ denotes p<0.05 for treatment with rAAV9-shPLB vs. rAAV9-shGFP control group.

**D:** *Echocardiographic Changes During RNAi Therapy.* The figure shows the echocardiographic data on cardiac morphology and function which corroborate the morphometric findings. The LV end-diastolic diameter (LVEDD) was significantly enhanced by TAB. This dilation was reduced to within the normal range after 3 months of treatment with rAAV9-shPLB (lane 5), whereas the effect of 1 month of therapy with AdV-shPLB was also significant but less pronounced. Corresponding to the morphometric changes noted in panel C, the LV anterior and posterior wall thickness measured by echocardiography were significantly reduced (lanes 3, 5) compared to the heart failure groups after TAB and treatment with the control vectors (lanes 2, 4) (addendum to **Fig. 3*d***).

¶ denotes p<0.05 for animals treated with AdV-shPLB vs. control vector AdV-shGFP, ‡ denotes p<0.05 for treatment with rAAV9-shPLB vs. rAAV9-shGFP control group.

**E:** Cardiac BNP mRNA expression levels quantitated by *TaqMan*™ PCR in the different groups were consistent with the hemodynamics as shown in panels A and B.

¶ denotes p<0.05 for animals treated with AdV-shPLB vs. control vector AdV-shGFP, ‡ denotes p<0.05 for treatment with rAAV9-shPLB vs. rAAV9-shGFP control group.

**Supplemental Fig. 4**

**Cardiomyocyte miRNAs during RNAi Treatment**

**A:** There was no evidence of significant alteration of the levels of miRNAs 1 or 133a during treatment of NRCMs with any of the RNAi vectors described in this study at the given doses.

**B:** In contrast, several cellular miRNAs were strongly reduced in the presence of an hypertrophy-inducing drug despite otherwise unchanged culture conditions. In the presence of phenylephrine (PE) there was a marked reduction of miRNA-1 and miRNA-133a on day 5 of treatment with PE ± RNAi vector, consistent with previous studies by others. Treatment with the RNAi vectors AdV-shPLB or rAAV6-shPLB, respectively, was associated with elevation of these miRNA levels to baseline range.

¶ denotes p<0.05 for untreated (NT) *vs.* PE-treated cells, ‡ p<0.05 of cells treated with PE alone *vs.* PE + AdV-shPLB, † p<0.05 of PE *vs.* PE + rAAV6-shPLB.

**C:** Quantitation of cardiac miRNA1 and miRNA-133a levels in rats during RNAi treatment with either the adenoviral or the rAAV9 vector system showed a significant decrease of both miRNAs in the HF groups (treated with the shGFP control vectors) compared to sham, whereas both miRNA-1 and 133a were significantly elevated as compared to these groups in TAB rats treated with shPLB vector.

**Supplemental Table**

We have extensively used this model of pressure-overload hypertrophy in transition to heart failure over the last decade and have characterized the time course of heart failure development in previous publications (Miyamoto *et al.* Proc Natl Acad Sci USA 2000; 97: 793-798 - Table 1). The same model was used in this specific study on RNA interference therapies. The table shows the development of echocardiographic parameters up to 23 weeks after transaortic banding (TAB) compared to sham surgery. We have definitely observed the phenomenon that animals with TAB that survive beyond 22-24 weeks seem to stabilize somewhat at these low hemodynamic numbers. Probably they can only survive if they are able to sustain this level of hemodynamic numbers, otherwise they die.

A steady state of cardiac morphology and function was apparently also reached within the short-term follow-up phase of 1 month after injection of the RNAi vectors, since no significant further deterioration of cardiac function occurred between the control group of the long-term experiment (rAAV9-shGFP) vs. the control group of the short-term study (AdV-shGFP).

**Suppl. Fig. 1a-c : Suppression of shRNA Production by CMV Promotor in RNAi Vectors Carrying a GFP Expression Cassette**

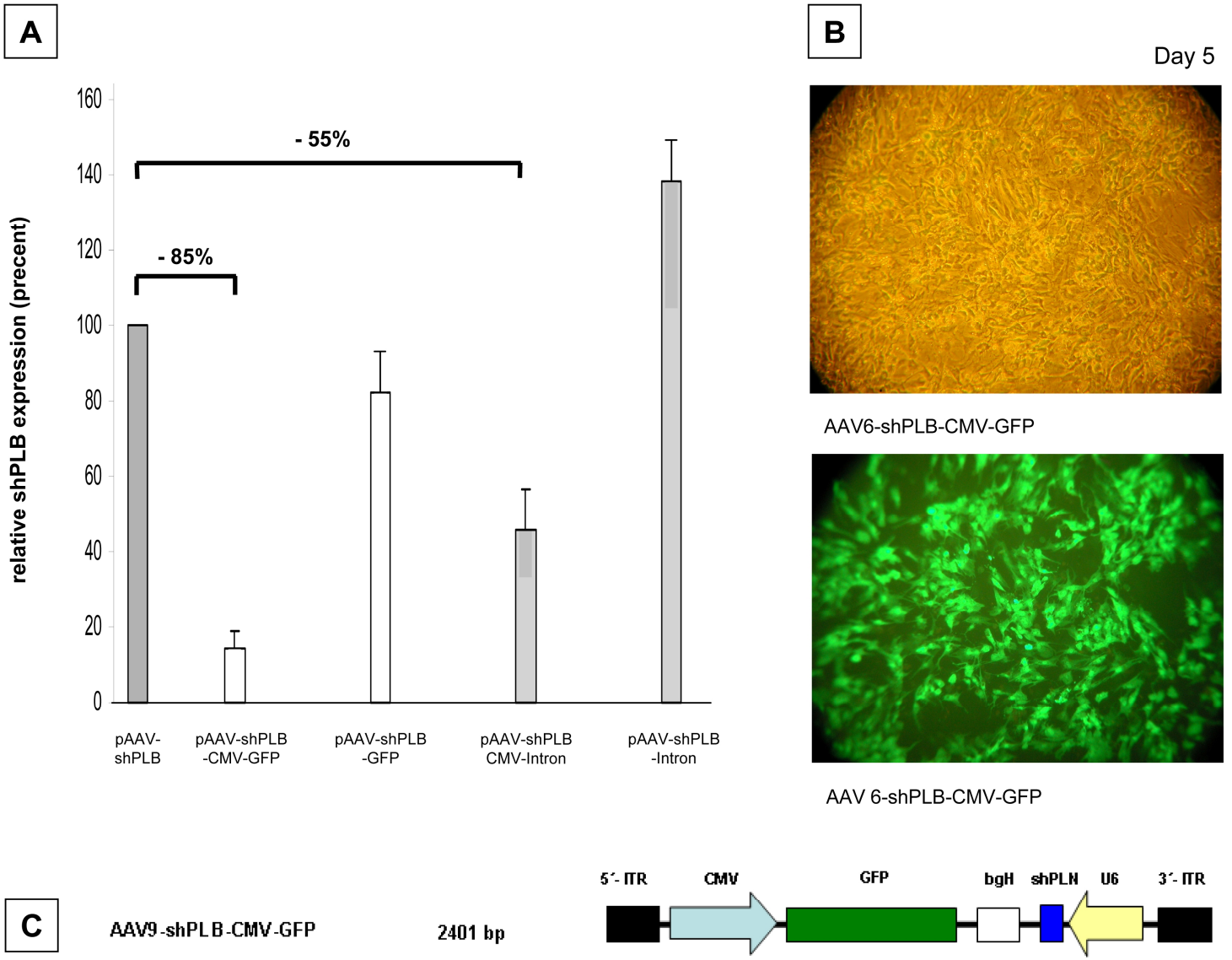

**Suppl. Fig. 1d,e : Alteration of Calcium Homeostasis in NRCMs During RNAi Treatment**

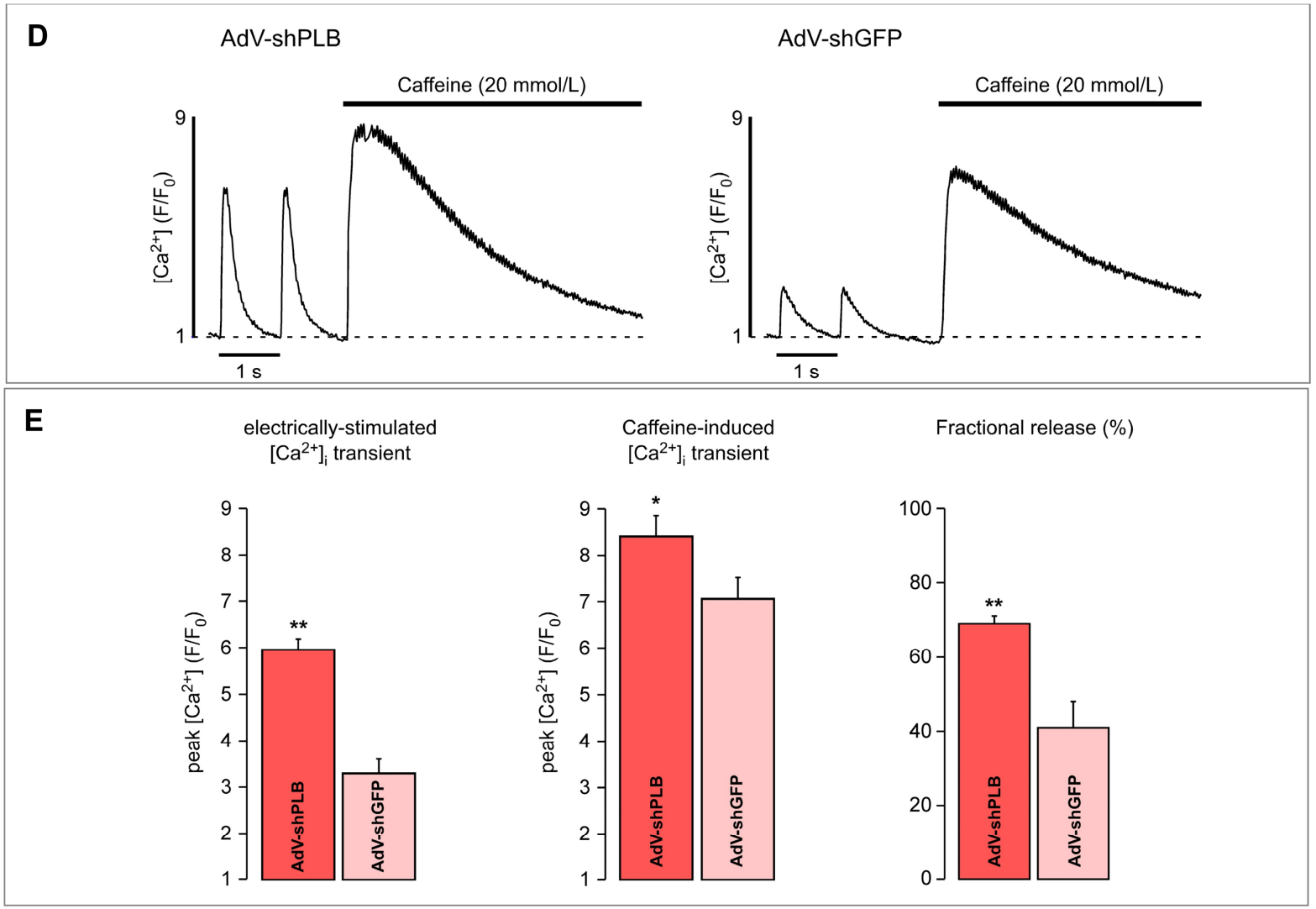

**Suppl. Fig. 2a : Cardiac GFP expression 1 month after intravenous (i.v.) rAAV9-GFP injection**

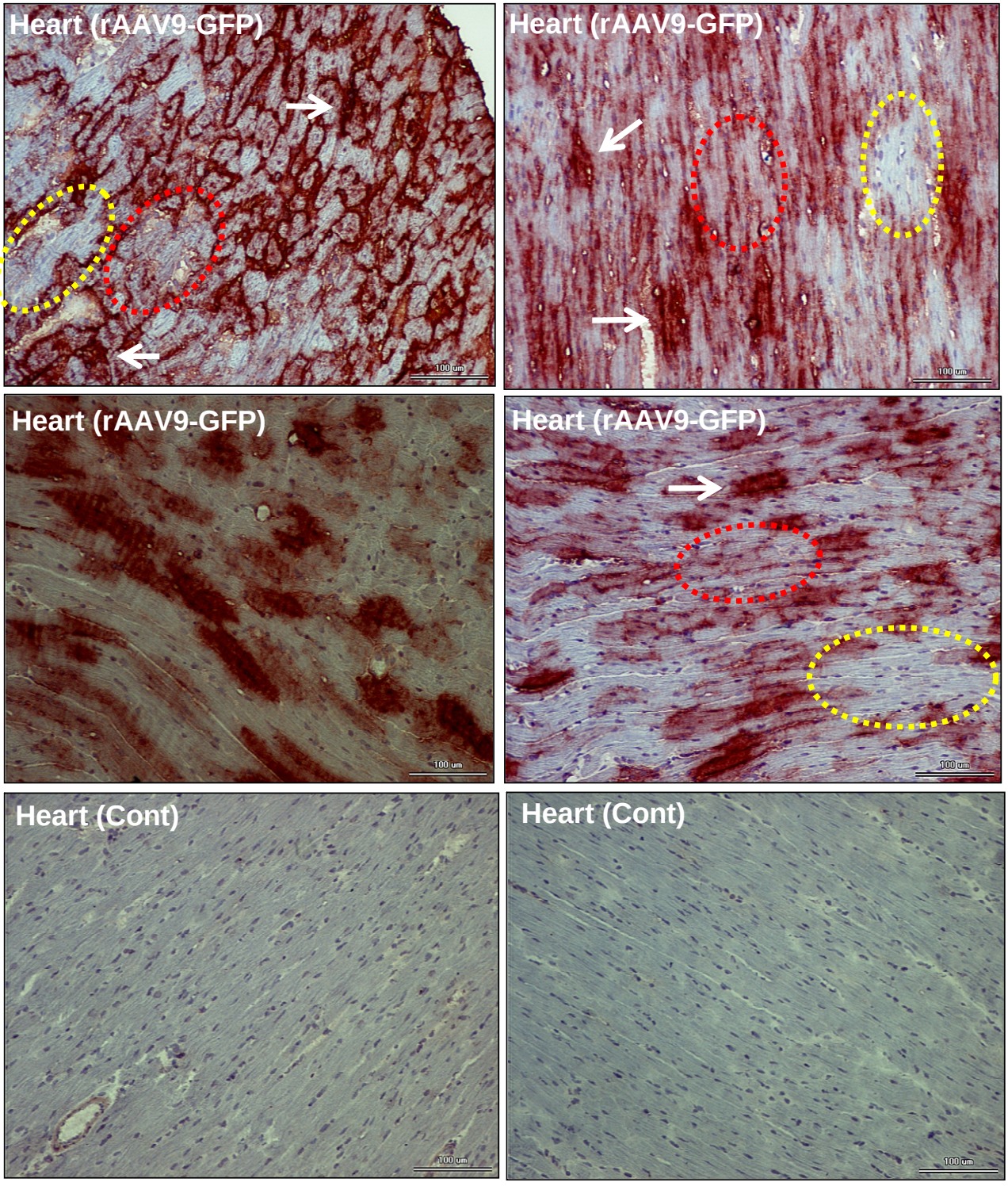


**Four upper panels (rAAV9-GFP) with primary GFP antibody, two lower panels (Cont) without.**

**Suppl. Fig. 2b : GFP expression in other organs 1 month after i.v. rAAV9-GFP injection**

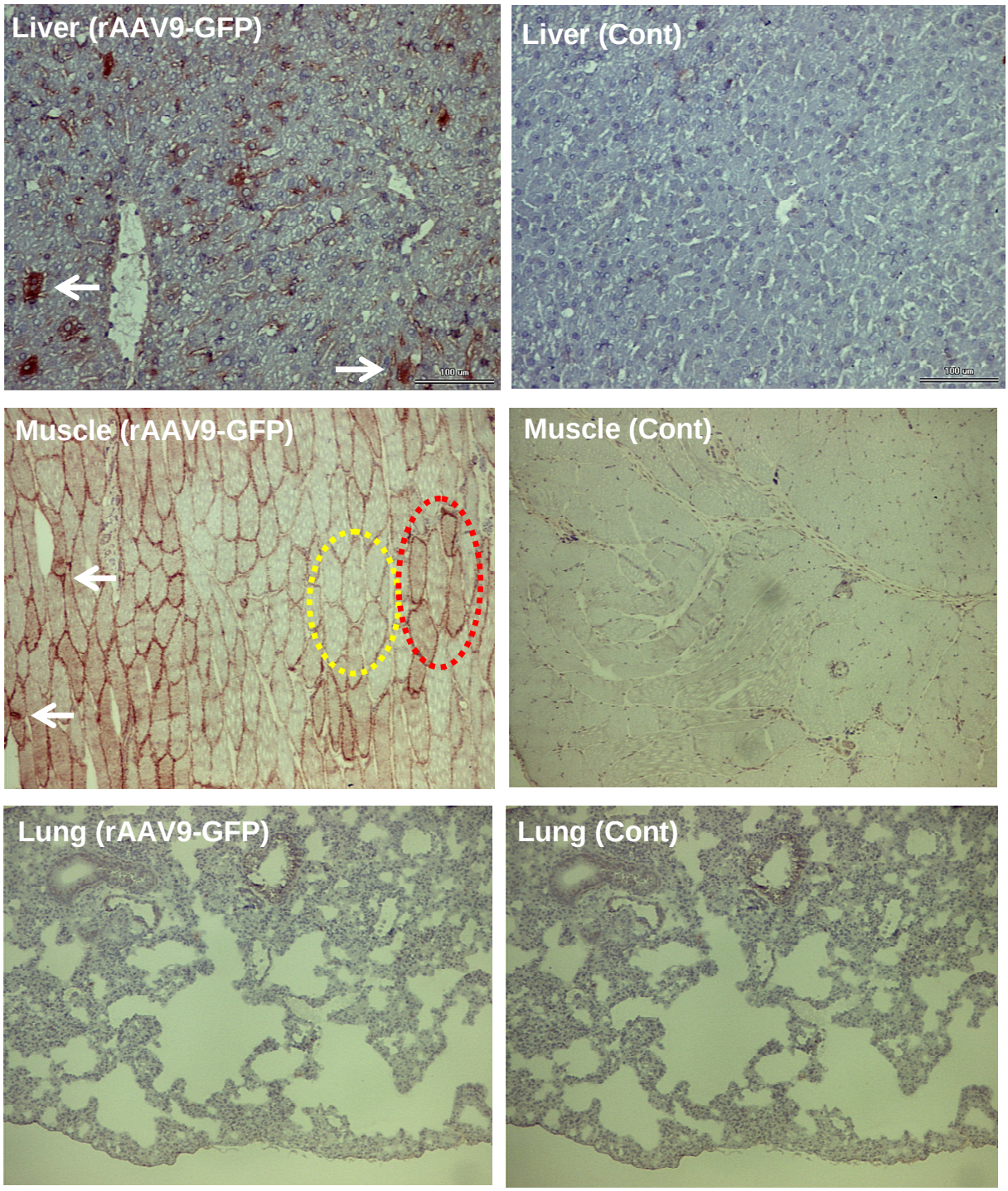


**Left panels (rAAV9-GFP) with primary GFP antibody, right panels (Cont) without.**

**Suppl. Fig. 2c : GFP quantitation by immunoblot in different organs after i.v. rAAV9-GFP injection**

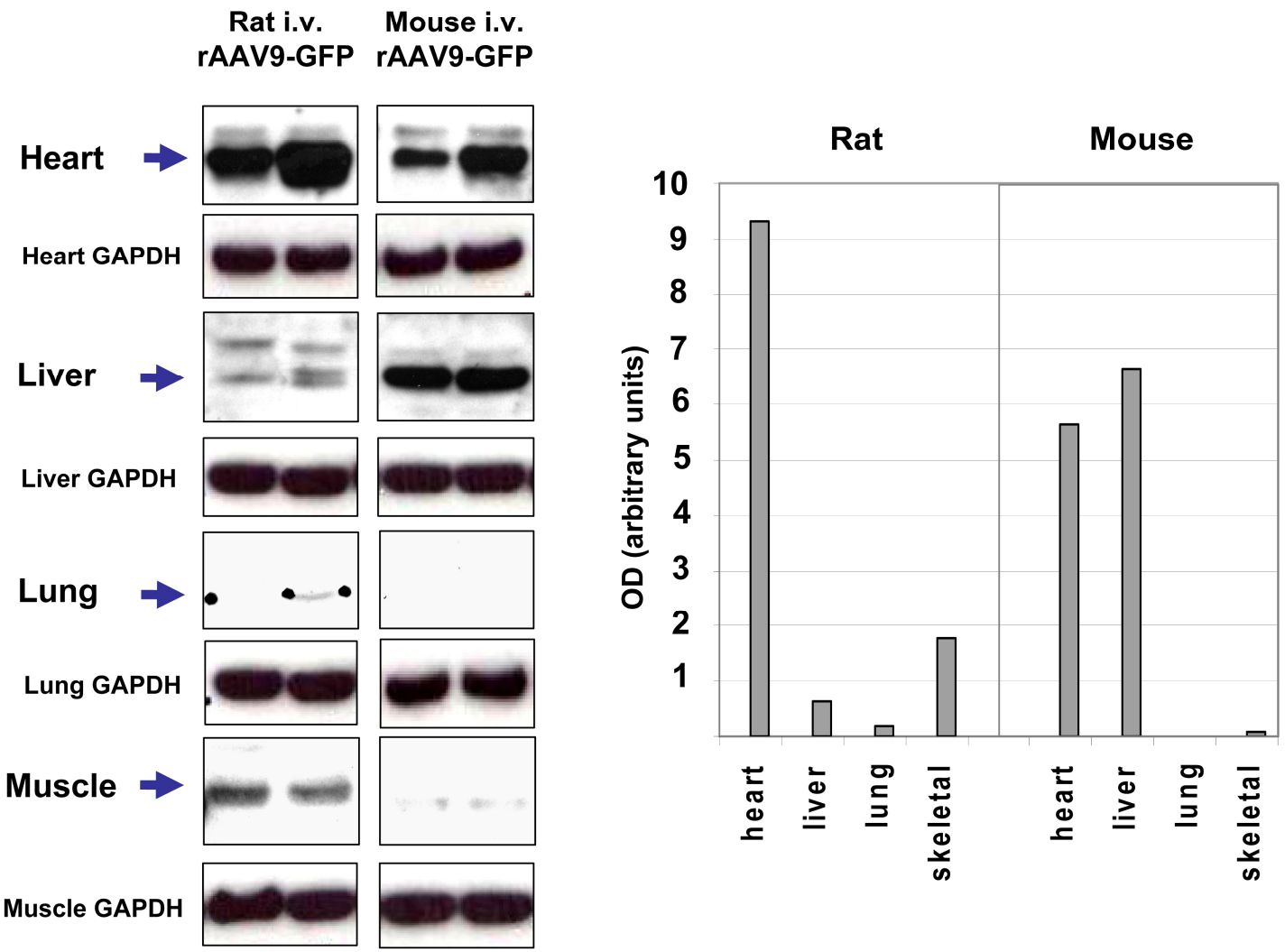

**Suppl. Fig. 3a : Influence of RNAi Therapy on Diastolic Function**

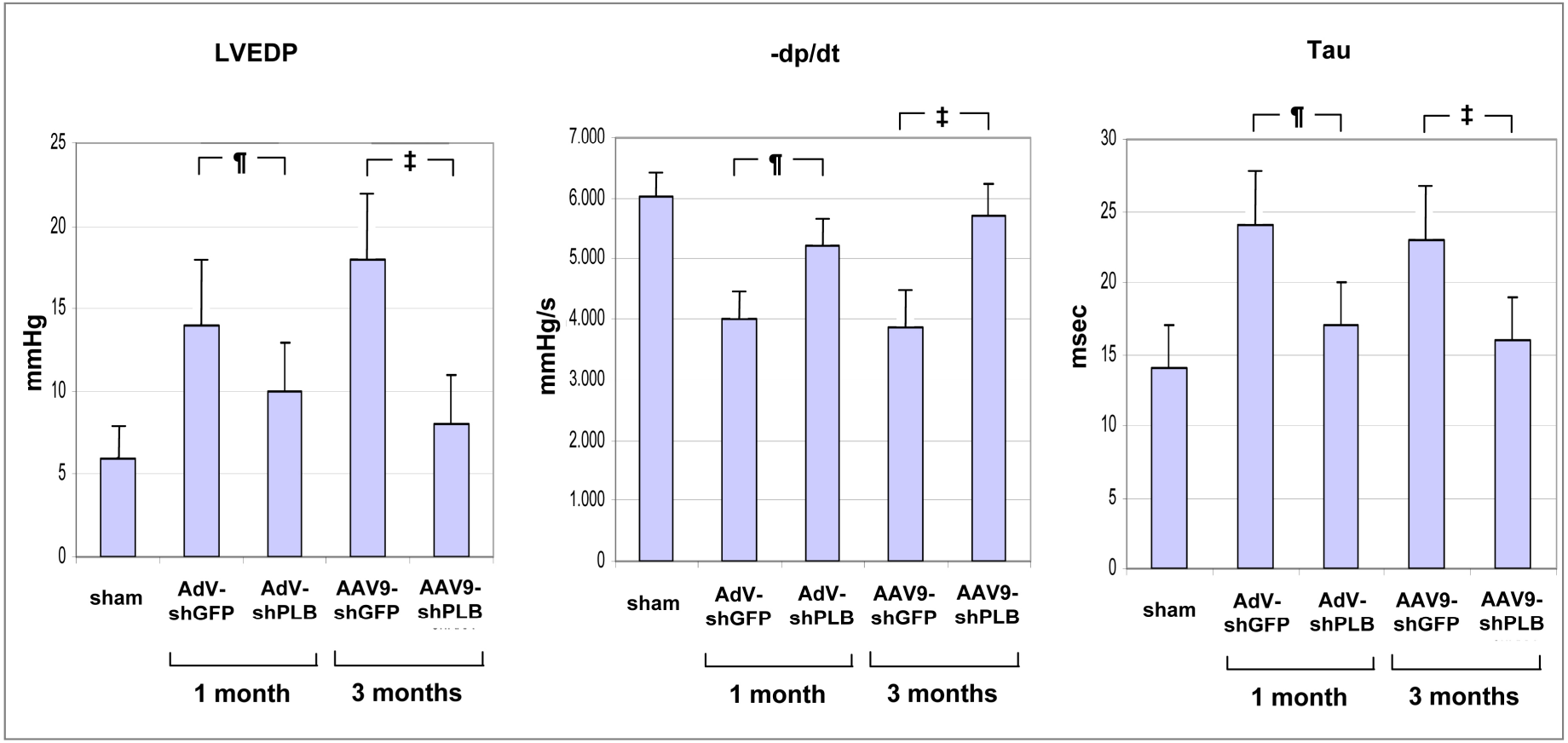


‡ : $p < 0.05$ for AAV9-shGFP vs. AAV9-shPLB

¶ : $p < 0.05$ for AdV-shGFP vs. AdV-shPLB

**Suppl. Fig. 3b : Influence of RNAi Therapy on Systolic Function**

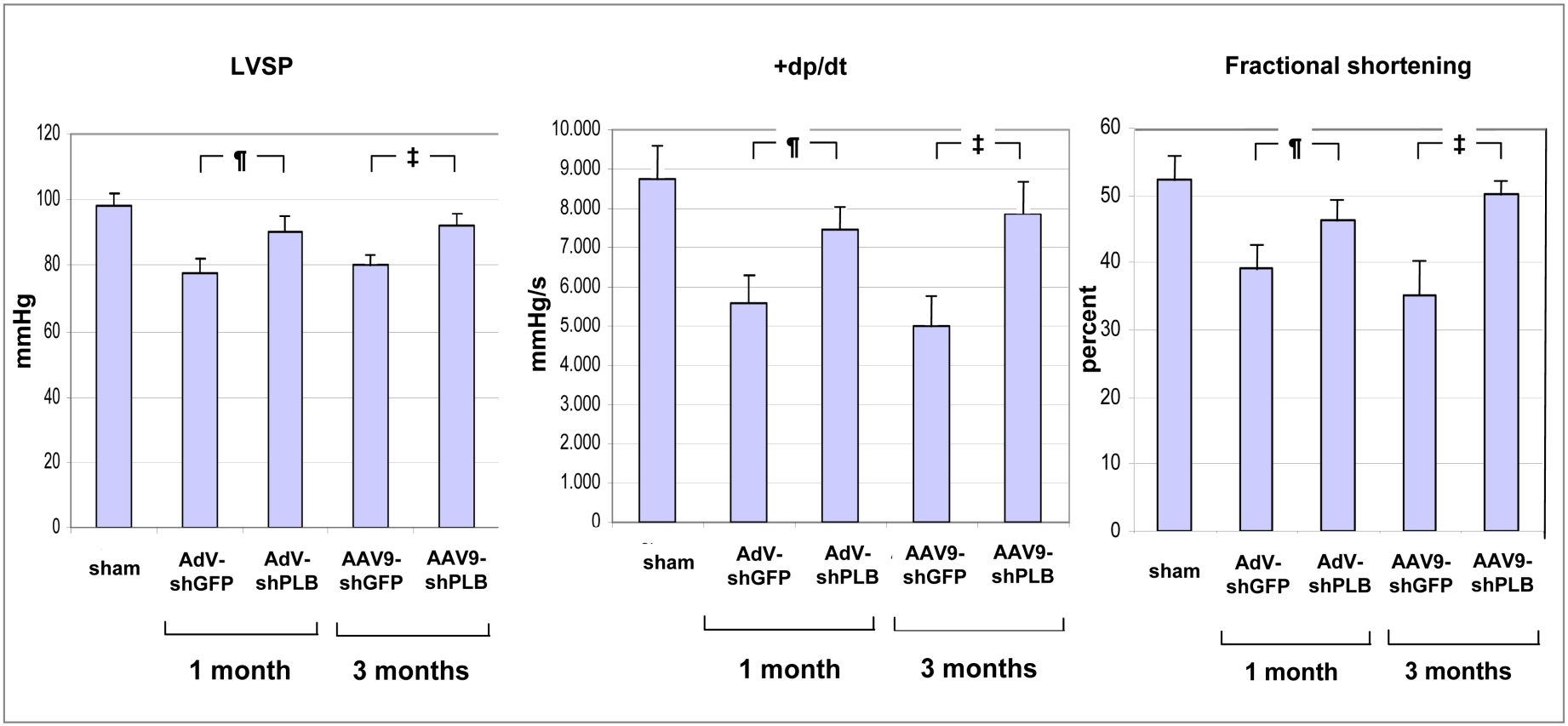


‡ : $p < 0.05$ for AAV9-shGFP vs. AAV9-shPLB

¶ : $p < 0.05$ for AdV-shGFP vs. AdV-shPLB

**Suppl. Fig. 3c : Morphometric Changes During RNAi Therapy**

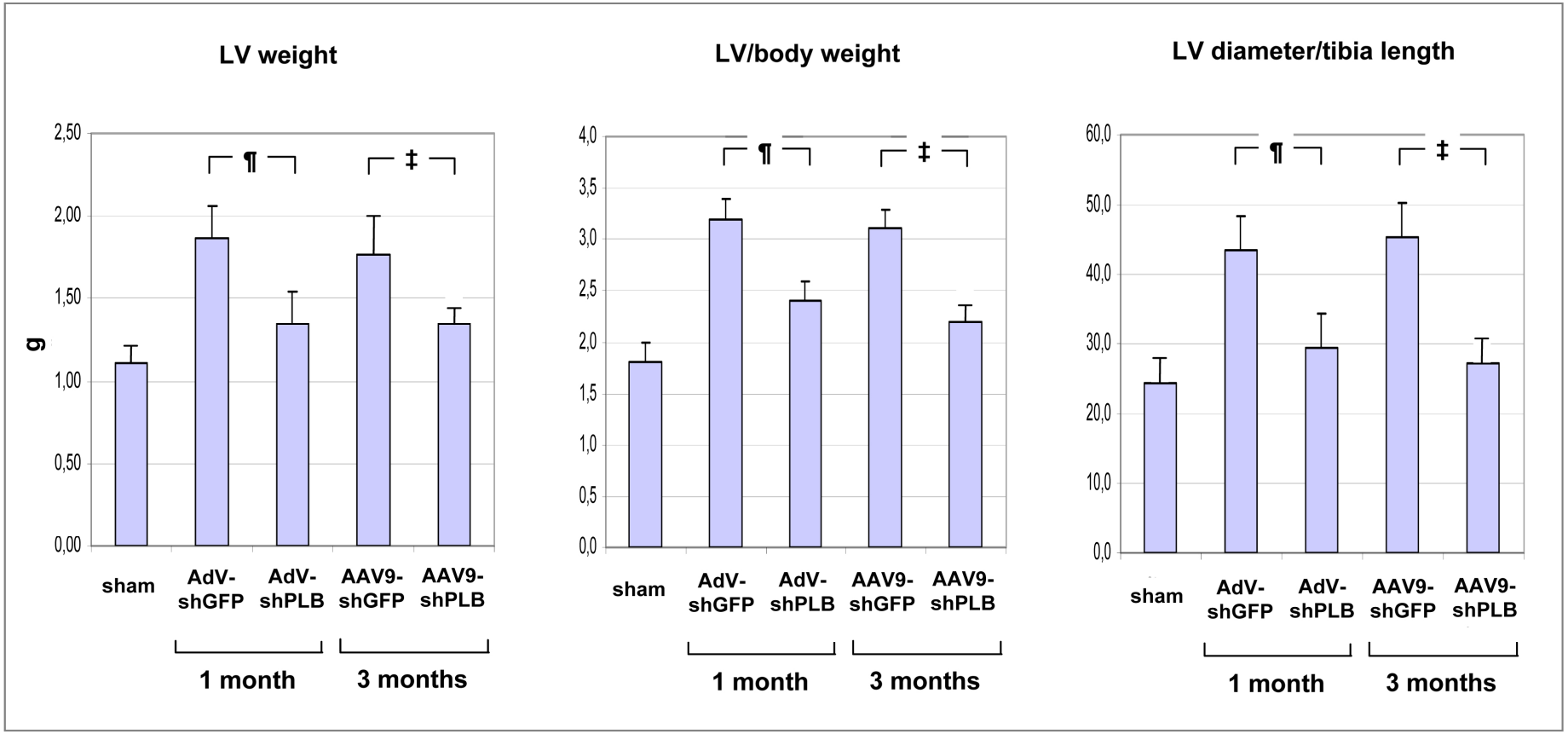


‡ : p < 0.05 for AAV9-shGFP vs. AAV9-shPLB

¶ : p < 0.05 for AdV-shGFP vs. AdV-shPLB

**Suppl. Fig. 3d : Echocardiographic Changes During RNAi Therapy**

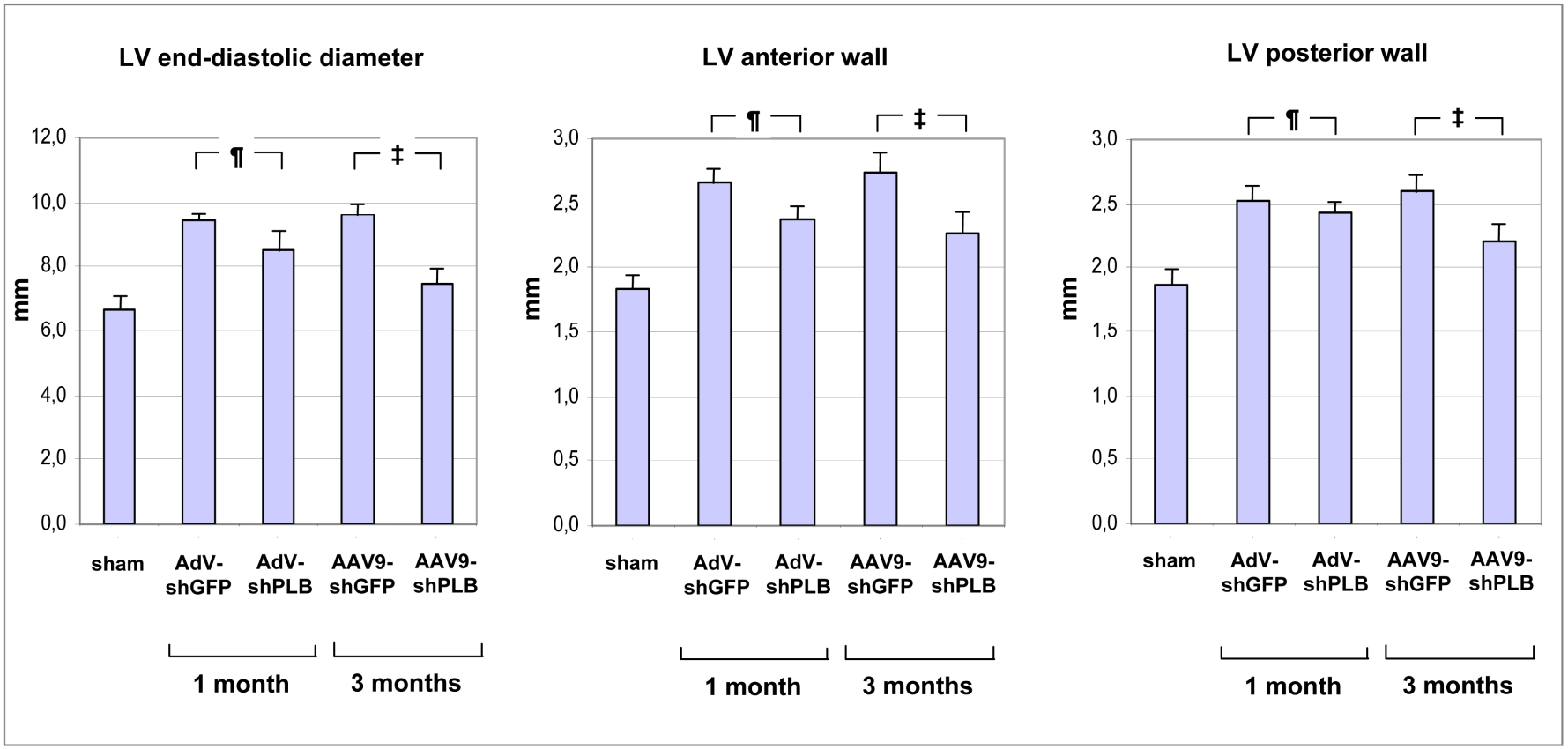


‡ : p < 0.05 for AAV9-shGFP vs. AAV9-shPLB

¶ : p < 0.05 for AdV-shGFP vs. AdV-shPLB

**Suppl. Fig. 3e : Cardiac BNP mRNA level during RNAi therapy**

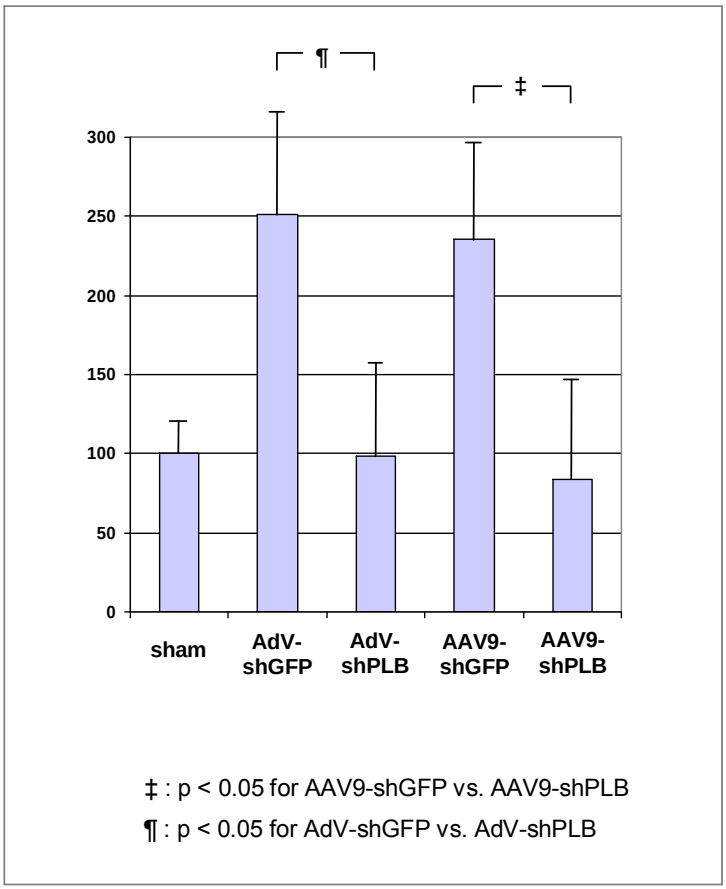

**Suppl. Fig. 4a,b : miRNA Levels in Cardiomyocytes Treated with RNAi Vectors**

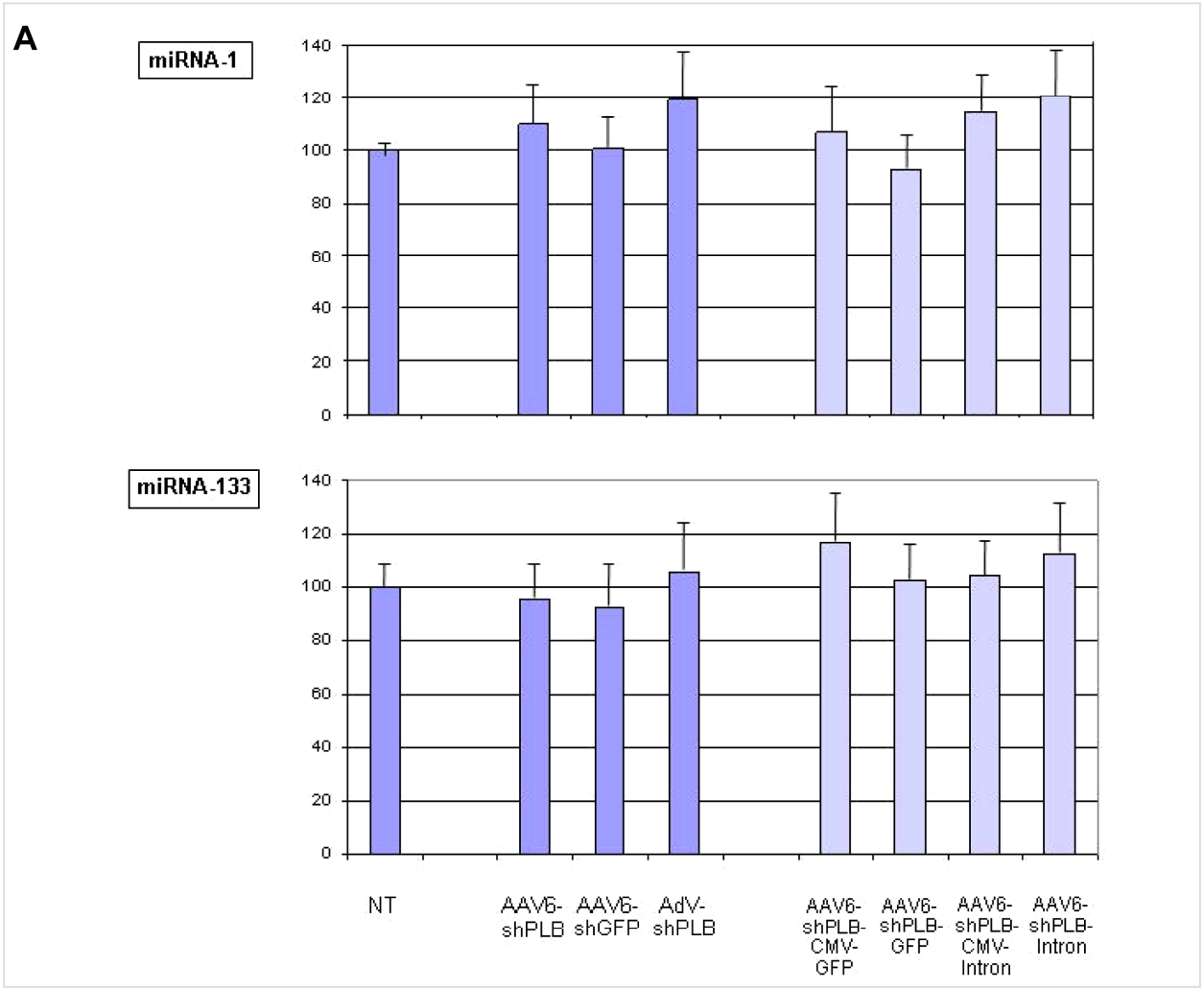


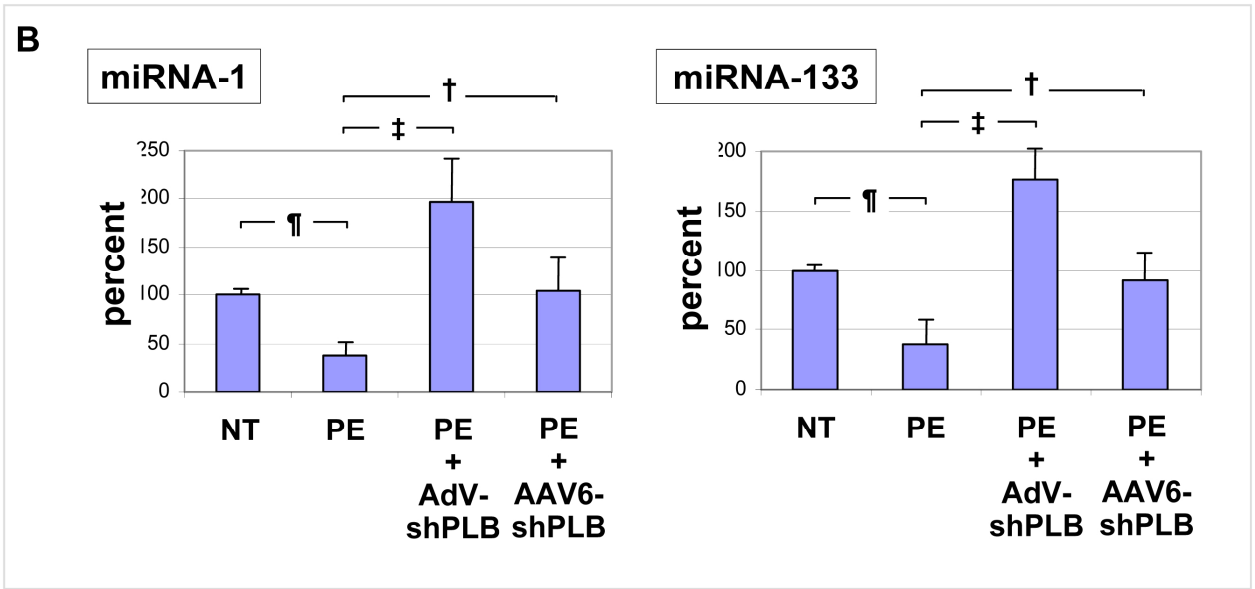

**Suppl. Fig. 4c: Cardiac miRNA-1 and 133 levels during RNAi therapy**